SEARCH FOR EXOTIC PROCESSES AT THE CERN $p\bar{p}$ COLLIDER

The UA2 Collaboration

Bern - CERN - Copenhagen(NBI) - Heidelberg - Orsay (LAL)
Pavia - Perugia - Pisa - Saclay (CEN)

Presented by Reza ANSARI
LAL-Orsay

ABSTRACT

The total UA2 data sample at the CERN $p\bar{p}$ Collider corresponds to an integrated luminosity of 910 nb^{-1}. Limits on various hypothetical processes , such as production of excited electrons , additional charged or neutral vector bosons , or supersymmetric particles , are presented from the analysis of this sample.

1. INTRODUCTION

The UA2 detector at the CERN $p\bar{p}$ collider has collected data over a period of four years, corresponding to integrated luminosities of 142 nb^{-1} at $\sqrt{s}$ = 546 GeV and of 768 nb^{-1} at $\sqrt{s}$ = 630 GeV. Using this data sample, we report on a search for hypothetical new particles, so-called "exotic" particles, which are predicted to be produced at the CERN $p\bar{p}$ collider with observable rates, by many theoretical models.

In section 2, we summarize the relevant features of the UA2 data analysis and event samples. We present limits on excited electrons, e^*, via the decay $W \to e^*\nu \to e\gamma\nu$, in section 3. In section 4, through the decays $Z \to \tilde{e}\tilde{e}$ and $Z \to \tilde{W}\tilde{W}$, we set limits on the masses of the supersymmetric partners of the electron, $\tilde{e}$, and of the W boson, $\tilde{W}$. In sections 5 and 6, via the processes $p\bar{p} \to \tilde{q}\tilde{q}$, $\tilde{q}\tilde{g}$ and $\tilde{g}\tilde{g}$, we discuss limits on the masses of the supersymmetric partners of quarks, $\tilde{q}$, and gluons, g, in the case of an unstable or stable partner of the photon, $\tilde{\gamma}$ or photino. Finally, we set limits on the masses of possible charged, W', or neutral, Z', additional vector bosons, in section 7.

2. DATA ANALYSIS AND EVENT SAMPLES

The UA2 detector has been described in detail elsewhere [1]. The data presented here are obtained from various triggers :
a) single electron candidates are obtained from the **W triggers**, which select electrons or photons with transverse energies above 11 GeV,
b) electron pairs or photon pairs from the Z triggers, which select two electrons or photons separated in azimuth by at least 60° and with transverse energies above 6 GeV,
c) multijet events from the inclusive jet triggers, which select events with a summed transverse energy of at least 25 GeV in a 120° azimuthal slice of the central calorimeter.
These triggers are exclusively constructed from calorimeter signals. As a result, the W and Z triggers are dominated by hadronic final states. However, their efficiency at detecting electrons or photons is close to 100%.

We refer the reader to previous publications for the detailed description of the standard UA2 electron selection criteria [2-4], which are applied in the off-line analysis. They essentially require a good matching between a track segment, reconstructed in the tracking chambers, a large signal in the preshower detectors, and an energy deposition in the calorimeters, compatible with that expected from an electromagnetic shower. In the forward/backward region, the presence of the magnetic field is used, to require in addition good matching between the measured momentum and energy. The global efficiency, ε_e, of these electron cuts was measured to be (73 ± 7)% from the $W \to e\nu$ analysis. This result was obtained for electrons of energy above 30 GeV. For lower values of the electron energy, we have two independent evaluations of the selection efficiency :
a) test beam data show that the efficiency for 5 to 20 GeV electrons should be 80 to 90% of that for 40 GeV electrons,
b) a study of low-mass electron pairs, where we expect to observe a significant contribution from the Drell-Yan continuum, has led us to conclude that the efficiency of the standard cuts for 10 GeV electrons is only (60 ± 15)% of that for 40 GeV electrons.
We have established that this discrepancy between the test beam results and the data is entirely due to the cuts on the preshower detectors, and, when studying processes involving low energy electrons, we have therefore relaxed these cuts in the following way :
a) in the central region, the threshold on the preshower signal is decreased from 3 to 2 minimum ionizing particles, the maximum allowed distance between track impact and preshower signal is increased from 10 to 20 mm, and the isolation cut on the preshower signal is removed.
b) in the forward/backward region, where the rejection of the electron selection cuts against background from hadronic jets is higher than in the central region, the preshower cuts are relaxed completely.

This procedure eliminates most of the energy dependence of ε_e, and we have checked that relaxing the other electron cuts does not introduce any unexpected increase in the observed signal from Drell-Yan.

For similar reasons, the selection of photon candidates is less strict than that of a previous analysis of single isolated photons [5]; in particular, most of the photon isolation criteria are relaxed, and the global efficiency, ε_γ, for identifying a photon is 50%. Half of the inefficiency arises from the 30% probability that a photon fails to convert in the 1.5 radiation length thick converter situated in front of the preshower detectors.

For the analysis involving hadron jets (sections 5 and 6), we use the standard UA2 jet cluster algorithm [6]. We have restricted the sample to jets well contained in the UA2 central calorimeter ($|\eta| < 0.85$, where η is the pseudorapidity of the jet axis). The response of the UA2 central calorimeter has been studied in great detail over the past years [6], and the effects of fragmentation and detector response on the parton energies have been included in the Monte-Carlo simulation.

3. SEARCH FOR EXCITED ELECTRONS

Excited lepton states are expected in models in which leptons are composite particles [7]. In a previous publication [3], we reported results of a search for excited electrons in UA2 through the decay sequence :

$$W \rightarrow e^* \nu \rightarrow e\gamma\nu. \qquad (1)$$

In this section we extend this analysis to the full UA2 data sample, which consists of 5340 events containing at least one electron candidate with transverse momentum above 11 GeV/c [4]. Of these events, only 24 contain also a photon candidate with transverse momentum above 10 GeV/c. These events are compatible with background from jet pairs, where one jet fakes an electron and the other jet fakes a photon. In addition, if we require that the missing transverse momentum be larger than 10 GeV/c, none of these events survives, whereas more than 95% of the events originating from process (1) survive (the exact number depending upon the mass of the excited electron).

To interpret this result, we have performed a Monte-Carlo simulation of this process in the UA2 detector. We have taken the assumption that the W couples to the transition magnetic moment of the e^*-ν current [8], thus producing an effective Lagrangian, which conserves gauge invariance, and can be written as :

$$L = (g/\sqrt{2})(\lambda/M^*)\, W_\alpha\, e^*\, \sigma^{\alpha\beta}\, q_\beta\, \nu_L + \text{h.c.} \qquad (2)$$

where g is the SU(2) coupling constant, λ represents the coupling strength, and M^* is the mass of the excited electron. The assumptions used to derive expression (2) for the Lagrangian have also been used in a search for excited leptons in e^+e^- collisions [9].

From the Monte-Carlo simulation, we extract the ratio $R(M^*)$ of the accepted cross-section for process (1) to the cross-section, σ, for the process $p\bar{p} \rightarrow W \rightarrow e\nu$, as a function of M^* and using $\lambda = 1$. The number N^* of expected events is then :

$$N^* = \lambda^2\, R(M^*)\, \sigma\, L\, \varepsilon_e\, \varepsilon_\gamma \qquad (3)$$

where $\sigma = 0.57$ nb [10], $L = 910\ \text{nb}^{-1}$ is the total integrated luminosity and ε_e, ε_γ are the electron and photon selection efficiencies quoted in section 2. We have included in the geometrical acceptance for process (1) the effect of the granularity of the UA2 calorimeter, which requires a minimum opening angle of 20° between an electron and a photon to separate efficiently the two energy clusters.

From the absence of candidates for process (1), we extract a 95% confidence region in λ-M^* space (using equation (3) with $N^* = 3$) for which the existence of excited electrons is excluded. This region is shown in Fig. 1 with the most recent and stringent limits from e^+e^- data [9,11].

It should be noted that the Lagrangian of equation (2) contains only chiral fields and assumes CP-invariance. Given these assumptions, limits on excited electron masses from (g-2) values are weaker than those shown in Fig. 1 [12].

4. SEARCH FOR $\tilde{e}$ AND $\tilde{W}$ IN Z DECAYS

In this section, we study low-mass electron pairs as a possible signal for supersymmetric particles. More precisely, we consider the following processes :

$$p\bar{p} \rightarrow Z + ... \rightarrow \tilde{e}\tilde{e} + ... \rightarrow e\,e\,\tilde{\gamma}\tilde{\gamma} + ... \qquad (4)$$

where the $\tilde{\gamma}$ escapes detection (stable photino), and

$$p\bar{p} \rightarrow Z + ... \rightarrow \tilde{W}\tilde{W} + ... \rightarrow e\,e\,\tilde{\nu}\tilde{\nu} + ... \qquad (5)$$

where the $\tilde{\nu}$ escapes detection (stable $\tilde{\nu}$ or $\tilde{\nu} \rightarrow \nu\,\tilde{\gamma}$).

These processes are characterized by final states containing two electrons and missing transverse momentum. The data analysis is therefore performed using the total UA2 data sample from the Z triggers. As discussed in section 2, the electron cuts of the $W \rightarrow e\nu$ analysis are relaxed to obtain an efficiency independent of the electron energy. These cuts are however applied to both electron candidates, contrary to the Z analysis of Ref. 4, in order to reduce the dominant background from fake electron pairs at low values of the electron pair mass, M_{ee}. We obtain a total of 57 candidate electron pairs with $M_{ee} > 10$ GeV/c^2.

Fig. 2 shows the distribution of M_{ee} versus the projection, p_T^{η}, of the electron pair transverse momentum on the bisector of the azimuthal angle between the two electron momenta. The majority of the events are concentrated at small values of p_T^{η}, as expected from standard processes or background. However, in the case of processes (4) and (5), a large fraction of the events will appear at large values of p_T^{η}, as illustrated by the dashed area in Fig. 2, where about 75% of $Z \rightarrow \tilde{e}\tilde{e}$ and $Z \rightarrow \tilde{W}\tilde{W}$ decays observable in UA2 are expected. The quantity p_T^{η} was chosen to discriminate processes (4) and (5) from standard processes, because it is experimentally the best measured component of the electron pair transverse momentum, and also because the missing transverse momentum cannot be used in this kinematic range due to the incomplete coverage of the UA2 detector.

Of the 39 events from the UA2 Z sample [4], 21 remain in Fig. 2. Most of the remaining events are concentrated at mass values near the kinematic threshold, in a region still dominated by background. For the 36 events of Fig. 2 with $M_{ee} < 70$ GeV/c^2, we estimate the background to be (20 ± 1) events, using the same method as described in the Z analysis of ref. 4, which assumes that, in a two-jet event, the probability that one of the jets satisfies the electron selection criteria is independent of the fragmentation of the other jet. The signal from genuine electron pairs is therefore (16 ± 6) events. This number was used to extract the value, $\epsilon_e = (60 \pm 15)\%$, quoted in section 2 for 10 GeV relative to 40 GeV electrons.

We have simulated processes (4) and (5) in order to estimate their contribution to Fig. 2. We have then performed a likelihood fit to the distribution of Fig. 2, taking into account the expected contributions from background, from the Drell-Yan continuum, which is the dominant standard process allowed by our kinematic cuts and electron selection criteria, and from processes (4) and (5).

The limits obtained are shown in Figs. 3a and 3b as 90% confidence level contours in $M_{\tilde{e}}$ - $M_{\tilde{\gamma}}$ and $M_{\tilde{W}}$ - $M_{\tilde{\nu}}$ space respectively. The limits of Fig. 3a are valid for a stable photino and assume $\tilde{e}_L$ and $\tilde{e}_R$ to be degenerate in mass. The limits of Fig. 3b assume that the $\tilde{W}$ is a pure gaugino and that the branching ratio for $\tilde{W} \rightarrow e\tilde{\nu}$ is 33%. The proper helicity-conserving amplitudes were used for the $\tilde{W}$ decay [13]. The limits in Fig. 3a assume conservatively that $M_{\tilde{W}} > M_Z/2$, and the limits in Fig. 3b assume that $M_{\tilde{e}} > M_Z/2$.

To better understan the difference between the results of Figs. 3a and 3b, we can compute the ratios $R_e = \Gamma(Z \rightarrow \tilde{e}\,\tilde{e})/\Gamma(Z \rightarrow e\,e)$, and $R_W = \Gamma(Z \rightarrow \tilde{W}\,\tilde{W})/\Gamma(Z \rightarrow e\,e)$ [14,15]. For small $\tilde{e}$ and $\tilde{W}$ masses, $R_e \sim 0.5$, whereas $R_W \sim 9.2$. These numbers show that, in Z decays, $\tilde{W}$ are produced more abundantly than $\tilde{e}$, and explain the better mass limits obtained by UA2 for the $\tilde{W}$ case (Fig. 3b) as compared to the $\tilde{e}$ case (Fig. 3a).

The hatched areas of Figs. 3a and 3b show how the limits vary if we increase the expected Drell-Yan contribution by 50% to take into account the larger higher-order QCD corrections (K factors) expected for M_{ee} around 20 GeV/c^2 (K ~ 2) as compared to $M_{ee} = M_Z$ (K ~ 1.3). The most up-to-date results from searches for $\tilde{e}$ and $\tilde{W}$ at e^+e^- machines (PETRA and PEP) [16] are also shown in Figs. 3a and 3b. In the $\tilde{W}$ case, the UA2 results improve significantly on the e^+e^- limits.

5. SEARCH FOR $\tilde{q}$ AND $\tilde{g}$ IN THE CASE OF AN UNSTABLE PHOTINO

In hadronic machines, the dominant sources of supersymmetric particles are $\tilde{q}\tilde{q}$, $\tilde{q}\tilde{g}$ and $\tilde{g}\tilde{g}$ production [17]. In most models, the photino is expected to be much lighter than the $\tilde{g}$ and $\tilde{q}$. In this and the following section, we assume that the $\tilde{g}$ decays into $q\bar{q}\tilde{\gamma}$, and the $\tilde{q}$ into $q\tilde{g}$ (if $M_{\tilde{q}} > M_{\tilde{g}}$), or into $q\tilde{\gamma}$ (if $M_{\tilde{q}} < M_{\tilde{g}}$).

In this section, we consider the case of an unstable photino, which decays into $\gamma\tilde{H}$, where the nature of $\tilde{H}$ is different in the framework of global [18] and local [19] supersymmetry. The missing transverse momentum spectrum expected in the final state is much softer than that expected in the case of a stable photino (see section 6). The final state contains 2 photons, n jets (where n lies between 2 and 6 depending on the production subprocess and the $\tilde{q}$, $\tilde{g}$ masses) and small missing transverse momentum (from the 2 $\tilde{H}$).

In order to achieve a good rejection against the very large background expected from QCD processes, we have analysed the full UA2 data sample obtained from the Z triggers, selecting those events with at least two photon candidates of transverse momentum above 6 GeV/c each and of invariant mass above 10 GeV/c^2. We obtain a sample of 309 pairs of such photon candidates, most of which are single or multiple π^0's (see ref. 5 for a detailed discussion of backgrounds to single photons in the UA2 experiment). In general, these pairs are not accompanied by jets of large transverse momentum. In particular, we observe no event with a photon pair mass above 10 GeV/c^2 and two jets with transverse momentum larger than 10 GeV/c. This translates into an observed cross-section smaller than 12 pb at the 90% confidence level. The photon detection efficiency is taken to be 50% as quoted in section 2, and we have checked from the data themselves that it is not reduced by the presence of nearby jets if the angle between the photon and the jet is larger than 45°, (in the simulation, we require a minimum angle of 45° between the photons and the final state partons).

We have performed the Monte-Carlo simulation using the cross-sections of ref.19, a standard set of structure function parametrisations with Λ_{QCD} = 200 MeV [20] and the gluino fragmentation distributions suggested in [21]. As in ref.19, we assume that there are five flavours of $\tilde{q}$, all degenerate in mass. All decays are assumed to be isotropic and a simulation of the response of the UA2 central calorimeter to jets is included (see section 2).

We obtain production cross-sections which are 30% lower than those of the ISAJET program [22], but this difference is well within the theoretical uncertainties. The experimental cuts and the geometrical acceptance result in an overall efficiency ranging from 10^{-5} to 10^{-1}, when the $\tilde{q}$,$\tilde{g}$ masses increase from 10 to 60 GeV/c^2.

The results are shown in Fig. 4a as 90% confidence level contours in the $\tilde{g}$ versus $\tilde{q}$ mass plane. We exclude $\tilde{q}$ masses between 9 and 46 GeV/c^2 and $\tilde{g}$ masses between 15 and 50 GeV/c^2. Fragmentation effects and higher-order terms result in an uncertainty of a few GeV/c^2 on the limits in the regions of small $\tilde{g}$ and $\tilde{q}$ masses. The limits in the high-mass region are insensitive to the value of the photino mass, provided that it remains smaller than ~ 30 GeV/c^2. However, the limit on the $\tilde{q}$ mass goes down from 60 GeV/c^2 to 46 GeV/c^2 if the gluino mass increases from 100 GeV/c^2 to 1000 GeV/c^2, whereas the limit of 50 GeV/c^2 on the $\tilde{g}$ mass is unchanged if the $\tilde{q}$ mass becomes very large. Finally, we note that these results are not sensitive to the exact value of the photino lifetime if the average decay path in UA2 remains smaller than ~ 1 cm, which is the case for photino masses larger than 1 GeV/c^2 in the framework of global supersymmetry [17], and for all photino masses in the framework of local supersymmetry [18].

6. SEARCH FOR $\tilde{q}$ AND $\tilde{g}$ IN THE CASE OF A STABLE PHOTINO

We return now to the case where the photino is the lightest supersymmetric particle, and is therefore stable. In this case, hadronic production of $\tilde{q}$ and $\tilde{g}$ results in final states with two to six jets and missing transverse momentum, p_T^m. In contrast to section 5, where the requirement of two photons considerably reduces the hadronic background from multijet events, we have now to deal directly with this background, particularly since large p_T^m can be faked in UA2 by a jet escaping at polar angles θ smaller than 20° with respect to the beams, or depositing only a small fraction of its energy in the forward-backward calorimeters.

We are thus led to look for multijet final states with large p_T^m. We select an initial sample of 31075 two- or three- jet events, where each jet has a transverse energy above 12 GeV, and with at least one pair of jets with azimuthal separation $\Delta\phi$ such that :
a) $\Delta\phi < 95°$, to satisfy the single jet trigger threshold of 25 GeV (see section 2) and
b) $\Delta\phi > 15°$, to reject beam-halo background.
In the following, we call third jet a jet, which is present in the event in addition to the pair of jets, which passes these cuts. Of this initial sample, 1506 events have $p_T^m > 30$ GeV/c. In order to reject events, where a jet, entering the forward-backward calorimeter, has deposited only a small fraction of its energy, thus simulating a large value of p_T^m, we require in addition that :
a) the total energy deposited in the forward-backward calorimeters be less than 12 GeV and
b) the azimuthal separation between the vector sum of the central calorimeter jet transverse momenta and the vector sum of the forward-backward calorimeter cell transverse energies be less than 135°.
These cuts reduce the sample to 203 two- or three-jet events with $p_T^m > 30$ GeV/c.

This large number of events does not allow us to exclude possible $\tilde{q}$ or $\tilde{g}$ production. We therefore retain only three-jet events, with $p_T^m > 30$ GeV/c. Of the thirteen events which remain, after applying the cuts described above, twelve events have similar configurations, where the third jet is the jet of largest transverse energy. Such configurations are not expected in supersymmetric processes, and we therefore require that this third jet have transverse energy less than 40 GeV. After this last cut one event remains, which is identified as a $W \rightarrow e\nu$ decay accompanied by two jets (one of the three jets is in fact an electron).

This analysis leads to an observed cross-section of less than 8 pb at the 90% confidence level, from which we can extract limits in the $M_{\tilde{g}}$ - $M_{\tilde{q}}$ plane, as shown in Fig. 4b. Because of the more stringent kinematic cuts applied than in the case of an unstable photino, the limits of Fig. 4b are not as

good as the ones of Fig. 4a. Neither are they as good as the most recent preliminary limits from UA1 [23], due to the better coverage in polar angle of the UA1 detector. We recall that, in the stable photino case, a lower limit $M_{\tilde{q}} > 23$ GeV/c² is obtained from experiments at PETRA [11], as shown in Fig. 4b.

7. SEARCH FOR ADDITIONAL VECTOR BOSONS

Additional vector bosons arise naturally in the framework of many possible extensions of the minimal $SU(2)_L \times U(1)$ standard model of electroweak interactions, whether it be through right-handed currents [24], composite models [25], or various models derived from superstring theories [26]. Limits have been extracted on heavy Z bosons from neutral current data in the framework of specific models [27] and from a theoretical analysis of UA1 and UA2 data [28].

In the following, we extract general limits on additional charged or neutral vector bosons,as a function of their mass, $M_{W',Z'}$, their coupling to quarks, λ_q, and their branching ratio to electrons, B_e, where λ_q and B_e are normalized to the standard model values. We choose these variables, because the cross-section, σ, for the production of an additional vector boson and its subsequent electronic decay, is :

$$\sigma = \sigma_o . \lambda_q . B_e \, , \qquad (6)$$

where σ_o is the cross-section for standard couplings. We assume that :

$$\Gamma_{W',Z'} = \Gamma_{W,Z} \cdot M_{W',Z'} / M_{W,Z} \, , \qquad (7)$$

where $\Gamma_{W',Z'}$ and $\Gamma_{W,Z}$ are the widths of the additional and standard vector bosons respectively.

We have simulated W′ and Z′ production and decay in UA2, using the structure function parametrisation of ref. 29. We have then performed a likelihood fit to four data samples, using the electron transverse momentum spectrum, for the case of W′, and the invariant mass spectrum of the two electrons, for the case of Z′ :

1) for $M_{W'} > M_W$, we use the standard UA2 sample [4] of 251 $W \to e\nu$ candidates with electron transverse momentum, p_T^e, larger than 20 GeV/c and with an electron-neutrino transverse mass larger than 50 GeV/c². We recall that one $W \to e\nu$ candidate has a very large value of p_T^e, $p_T^e = 77$ GeV/c, which is unlikely for $W \to e\nu$ decays not accompanied by jets [4]. We also note that,for a W′ of mass 160 GeV/c² and with standard couplings, we should observe 15 events with p_T^e between 70 and 80 GeV/c,

2) for $M_{Z'} > M_Z$, we use the final UA2 sample [4] of 39 $Z \to e^+e^-$ candidates with $M_{ee} > 76$ GeV/c²,

3) for $M_{W'} < M_W$, we use a sample of 1300 electron candidates with $p_T^e > 12$ GeV/c and no jet activity at opposite azimuth to the electron. These events are dominated by background from jets, which fake the electron signature, and their estimated contribution is included in the likelihood fit. The results are not very sensitive to the exact knowledge of the background, since the expected signal from a light W′ is of the same order of magnitude,

4) for $M_{Z'} < M_Z$, we use the low-mass pair sample of Fig. 2, which contains 21 $Z \to e^+e^-$ candidates.

The results are shown in Figs. 5a and 5b, for W′ and Z′ respectively, as 90% confidence level contours in the $M_{W',Z'}$ versus $\lambda_q\lambda_e$ plane. In principle, we would be sensitive to additional W′ and Z′ almost degenerate in mass with the standard vector bosons, because they would result in observed rates for $W \to e\nu$ or $Z \to e^+e^-$ larger than the theoretical predictions. In practice, our cross-section measurements [10] and the theoretical predictions are subject to large uncertainties, thus precluding the

obtention of any significant limit. We also note that the mass limits of Figs. 5a and 5b are affected by an overall uncertainty of ± 5 GeV/c^2, due to the structure function uncertainties and to the uncertainty on the absolute electron energy scale.

An additional W′ with $M_{W'} < 25$ GeV/c^2 would have been seen at the ISR and at PETRA. Similarly, an additional Z′ with $M_{Z'} < 50$ GeV/c^2 would have been detected at PETRA. We therefore conclude from Figs. 5a and 5b that additional vector bosons with masses smaller than the standard ones are excluded for couplings to quarks and leptons similar to the standard model ones.

In the high mass region, we exclude a W′ with $M_{W'} < 209$ GeV/c^2 and a Z′ with $M_{Z'} < 180$ GeV/c^2, for standard couplings. We note, however, that, for $\lambda_q^2 B_e < 0.15$, no limit on the existence of additional W′ or Z′ can be obtained from our data. Most models derived from superstring theories [27] predict at least one extra Z boson with a reduced coupling to quarks, $\lambda_q^2 \sim 0.2$, and with B_e varying from 0.3 to 1.0 depending upon the masses of the new particles predicted by these models. Our data do not exclude any significant region in Fig. 5b for $\lambda_q^2 B_e$ values between 0.06 and 0.20.

8. CONCLUSIONS

The analysis of the total UA2 data sample has led to improved limits on various exotic processes, involving excited electrons, supersymmetric particles ($\tilde{e}$, $\tilde{W}$, $\tilde{q}$, $\tilde{g}$) and additional vector bosons. In particular, we exclude $\tilde{q}$ masses between 9 and 46 GeV/c^2 and $\tilde{g}$ masses between 15 and 50 GeV/c^2 in the case of an unstable photino. We also exclude additional W′ of masses less than 209 GeV/c^2 and additional Z′ of masses less than 180 GeV/c^2, if their couplings to quarks and leptons are the same as for the standard vector bosons, except if they are degenerate in mass with the standard W and Z.

REFERENCES

1. UA2 Collaboration. B. Mansoulié : The UA2 apparatus at the CERN $p\bar{p}$ Collider, Proc. of the 3rd Moriond Workshop on $p\bar{p}$ Physics (1983) p.609 : éditions Frontières 1983 ;
   A. Beer et al., Nucl. Inst. Meth. 224 (1984) 360 ;
   M. Dialinas et al., LAL – RT/83 – 14.

2. UA2 Collaboration. P. Bagnaia et al., Z. Phys. C24 (1984) 1.

3. UA2 Collaboration. J.A. Appel et al., Z. Phys. C30 (1986) 1.

4. UA2 Collaboration. R. Ansari et al., Phys. Lett. 186B (1987) 440.

5. UA2 Collaboration. J.A. Appel et al., Phys. Lett. 176B (1986) 239.

6. UA2 Collaboration. J.A. Appel et al., Z. Phys. C30 (1986) 341.

7. H. Terazawa et al., Phys. Lett. 112B (1982) 387.

8. A. De Rujula et al., Phys. Lett. 140B (1984) 253.

9. CELLO Collaboration. H.-J. Behrend et al., Phys. Lett. 168B (1986) 420.

10. UA2 Collaboration. R. Ansari et al., CERN-EP/87-48, 1987, to be published in Physics Letters.

11. S. Komamiya, International Symposium on Lepton and Photon Interactions at High Energies, Kyoto, Japan, 1985, Nissha Printing Co. Ltd.

12. F.M. Renard, Phys. Lett. 116B (1982) 264 ;
    S. Narison, Phys. Lett. 167B (1986) 214.

13. R. Budny, Phys. Rev. D14 (1976) 2969.

14. N. Cabibbo et al., Phys. Lett. 132B (1983) 195.

15. V. Barger et al., Phys. Rev. D28 (1983) 2912.

16. S. Whitaker, Proc. of Berkeley Conference, 1986, to be published.

17. S. Dawson et al., Phys. Rev. D31 (1985) 1581.

18. P. Fayet, Unification of the fundamental particle interactions, eds S. Ferrara, J. Ellis, P. Van Nieuwenhuizen (Plenum,New York,1980) 587.

19. J. Ellis et al., Nucl. Phys. B238 (1984) 453 ;
    H. Komatsu and J. Kubo, Phys. Lett. 157B (1985) 90 ;
    H.E. Haber et al., Phys. Lett. 160B (1985) 297.

20. E. Eichten et al., Rev. Mod. Phys. 56 (1984) 579 ; and Erratum, Rev. Mod. Phys. 58 (1986) 1065.

21. A. de Rujula and R. Petronzio, Nucl. Phys. B261 (1985) 587.

22. F. Paige and S. Protopopescu, BNL Report 31987 (1981).

23. UA1 Collaboration. J. Kroll, to be published in Proc. of the 22d Moriond Workshop on Electroweak Interactions (1987).

24. P. Langacker et al., Phys. Rev. D30 (1984) 1470.

25. U. Baur et al., MPI-PAE/PTh 29/85 (1985).

26. E. Cohen et al., Phys. Lett. 165B (1985) 76 ;
F. del Aguila et al., CERN-TH 4536 (1986) ;
D. London and J.L. Rosner, Phys. Rev. D34 (1986) 1530.

27. L.S. Durkin and P. Langacker, Phys. Lett. 166B (1986) 436 ;
F. del Aguila et al., CERN-TH 4376 (1986).

28. V.Barger et al., Phys. Rev. Lett. 56 (1986) 30.

29. D.W. Duke and J.F. Owens, Phys. Rev. D30 (1984) 49.

FIGURE CAPTIONS

1. Limits on excited electrons shown as 95% confidence level curves in λ - M^* space, where λ is the coupling strength and M^* the excited electron mass. Also shown are the most recent limits from e^+e^- experiments (CELLO at PETRA).

2. Distribution of electron-pair mass, M_{ee}, versus the best measured component of the electron pair transverse momentum, p_T^{η}, for a sample of 57 events containing 21 $Z \to e^+e^-$ candidates and 16 $\pm$ 6 Drell-Yan pairs after background subtraction. Also shown is the dashed area, where most of the electron pairs from $Z \to \tilde{e}\tilde{e}$ or $Z \to \tilde{W}\tilde{W}$ decays are expected.

3. a) In the case of a stable photino, limits on the $\tilde{e}$ and $\tilde{\gamma}$ masses obtained from the sample of Fig. 2 and shown as 90% confidence level contours. The dashed area illustrates the theoretical uncertainty on Drell-Yan production arising from higher-order terms (K-factors). Also shown (dashed curves) are the most recent limits from e^+e^- machines.
   b) With the assumptions quoted in the text, same as a) for the $\tilde{W}$ and $\tilde{\nu}$ masses.

4. a) In the case of an unstable photino, limits on the $\tilde{g}$ versus $\tilde{q}$ masses obtained from an analysis of photon pairs accompanied by jets and shown as 90% confidence level contours.
   b) In the case of a stable photino, same as a) obtained from an analysis of three-jet events with large missing transverse momentum.

5. a) Limits on an additional charged vector boson W′, obtained from an analysis of single electron candidates and shown as 90% confidence level contours in $M_{W'}$ versus $\lambda_q{}^2 B_e$ space, where $\lambda_{q'}$ the W′ coupling to quarks, and B_e, the W′ branching ratio to electron-neutrino, are normalized to the standard model values.
   b) Same as a) for an additional neutral vector boson Z′ from an analysis of electron pairs.

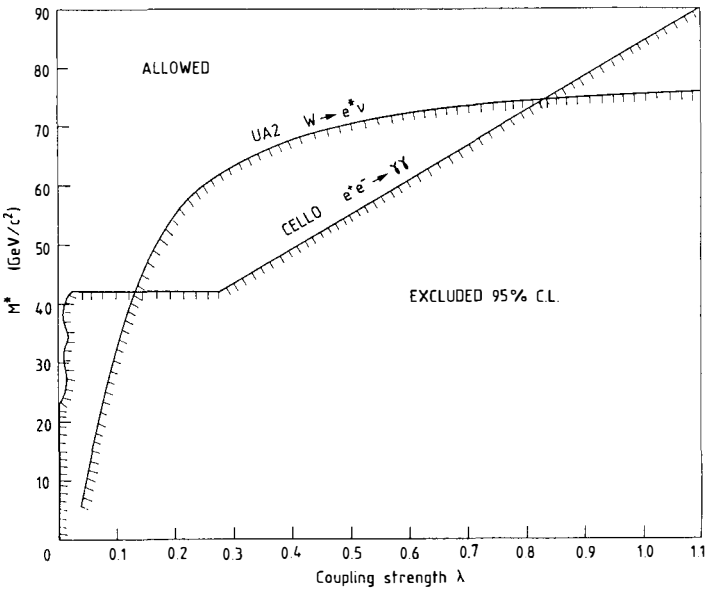
ALLOWED
UA2 W → e*ν
CELLO e⁺e⁻ → γγ
EXCLUDED 95% C.L.
M* (GeV/c²)
Coupling strength λ
0
10
20
30
40
50
60
70
80
90
0.1
0.2
0.3
0.4
0.5
0.6
0.7
0.8
0.9
1.0
1.1

Fig. 1

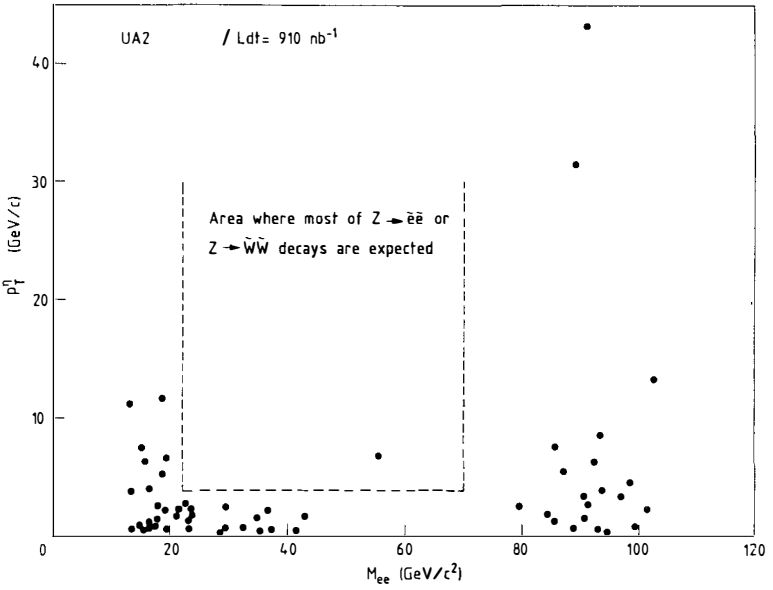
UA2
∫ Ldt= 910 nb⁻¹
Area where most of Z → ẽẽ or
Z → W̃W̃ decays are expected
p_T^0 (GeV/c)
M_ee (GeV/c²)
0
10
20
30
40
20
40
60
80
100
120

Fig. 2

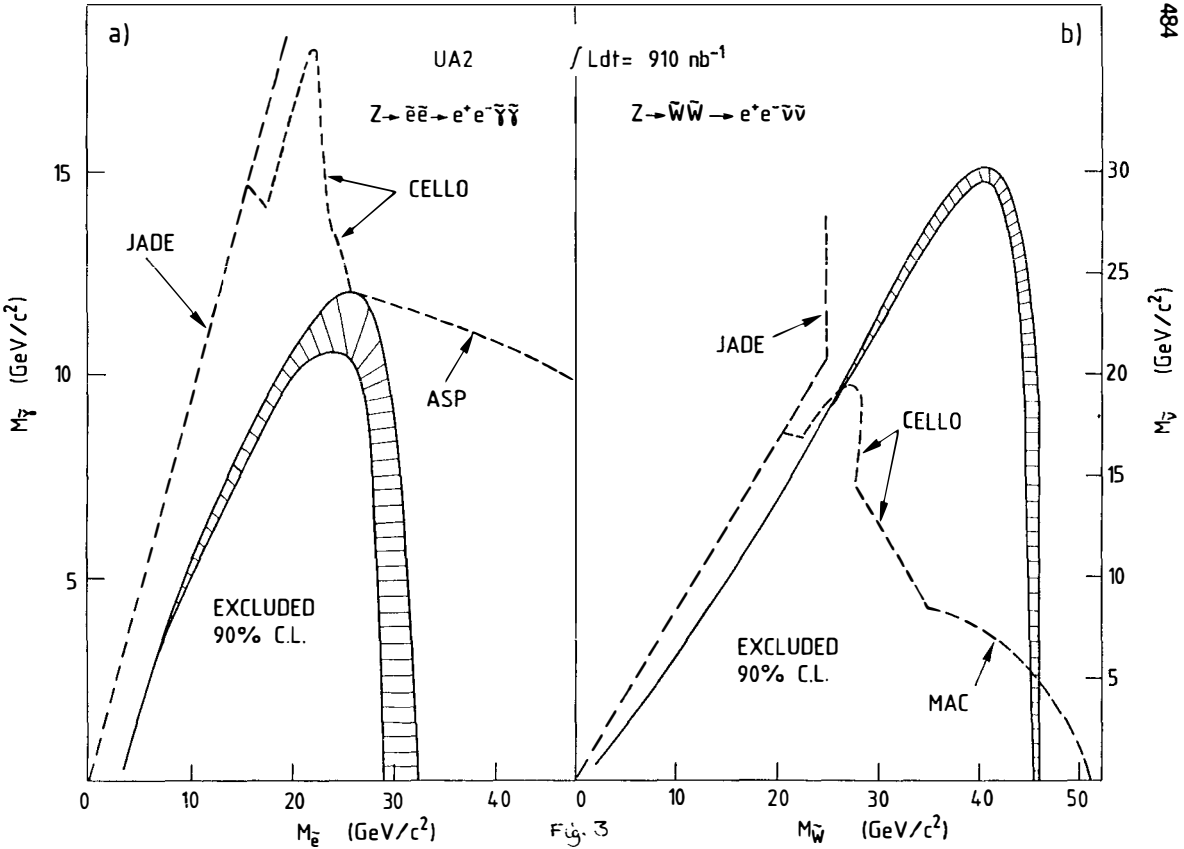
a)
UA2
∫ Ldt = 910 nb⁻¹
Z → ẽẽ → e⁺e⁻γ̃γ̃
CELLO
JADE
ASP
EXCLUDED
90% C.L.
M_γ̃ (GeV/c²)
M_ẽ (GeV/c²)
b)
Z → W̃W̃ → e⁺e⁻ν̃ν̃
JADE
CELLO
EXCLUDED
90% C.L.
MAC
M_γ̃ (GeV/c²)
M_W̃ (GeV/c²)

Fig. 3

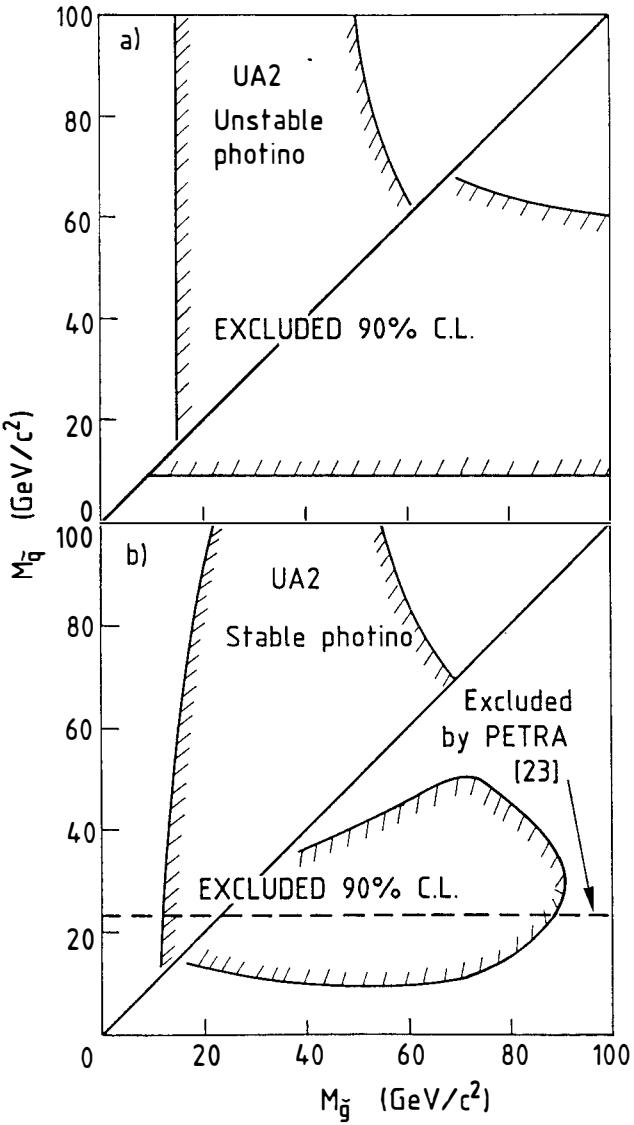
a)
UA2
Unstable
photino
EXCLUDED 90% C.L.
b)
UA2
Stable photino
Excluded
by PETRA
[23]
EXCLUDED 90% C.L.
$M_{\tilde{q}}$ (GeV/c^2)
$M_{\tilde{g}}$ (GeV/c^2)
0
20
40
60
80
100

Fig. 4

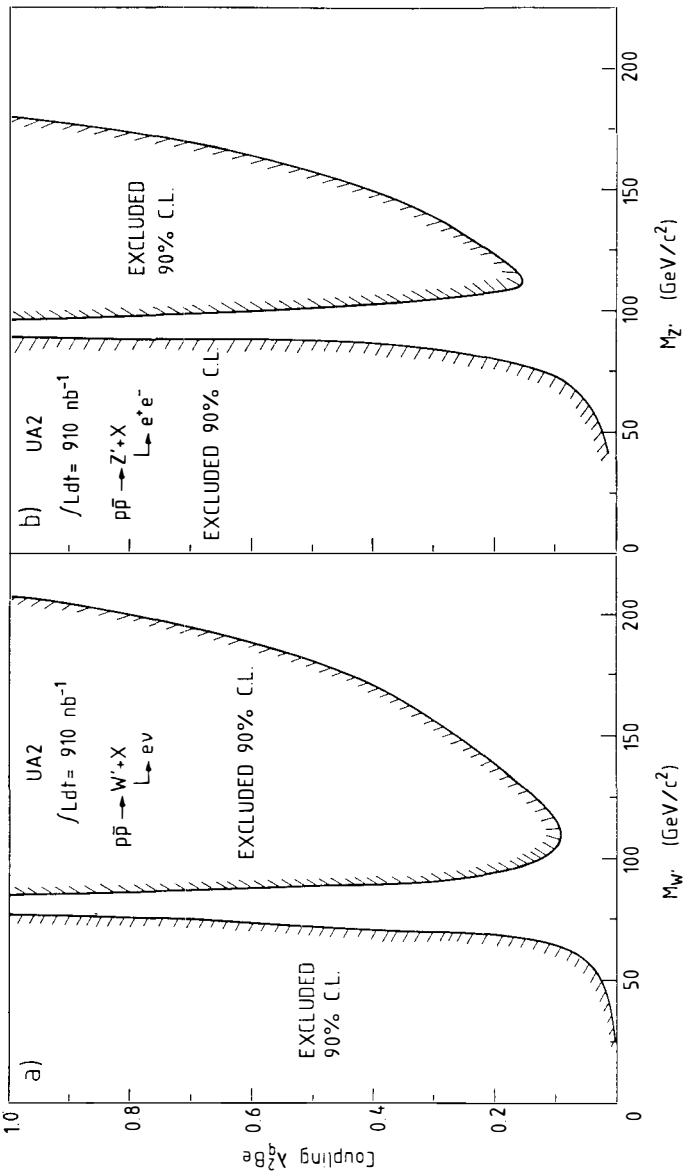
a)
UA2
∫Ldt= 910 nb⁻¹
p̄p → W'+X
↳ eν
EXCLUDED 90% C.L.
EXCLUDED
90% C.L.
b) UA2
∫Ldt= 910 nb⁻¹
p̄p → Z'+X
↳ e⁺e⁻
EXCLUDED 90% C.L.
EXCLUDED
90% C.L.
Coupling λ²qBe
1.0
0.8
0.6
0.4
0.2
0
50
100
150
200
M_W' (GeV/c²)
M_Z' (GeV/c²)

Fig. 5